Optimizing Electric Propulsion Systems for UAVs

Conference Paper · September 2008

DOI: 10.2514/6.2008-5916

2 authors, including:

Ohad Gur

29 PUBLICATIONS **361** CITATIONS

SEE PROFILE

12th AIAA/ISSMO Multidisciplinary Analysis and Optimization Conference
10 - 12 September 2008, Victoria, British Columbia Canada

AIAA 2008-5916

Optimizing Electric Propulsion Systems for UAV's

Ohad Gur[1] and Aviv Rosen[2]

Technion - Israel Institute of Technology, Haifa 32000, Israel

Design of an electric propulsion system for an Unmanned Aerial Vehicle (UAV) incorporates various disciplines such as: propeller's aerodynamic and structural properties, characteristics of the electric system, and characteristics of the vehicle itself. This makes the design of this propulsion system a Multidisciplinary Design Optimization (MDO) task. While the present propeller model is based on previous derivations that are described very briefly, new models of the electric motor and battery pack, which are based on examining existing products on the market, are described in more detail. The propeller model and a model of the electric system, together with various optimization schemes, are used to design optimal propulsion systems for a Mini UAV, for various goals and under various constraints. Important design trends are presented, discussed and explained. While the first part of the investigation is based on typical characteristics of the electric system, the second part includes a sensitivity study of the influence of variations of these characteristics on the optimal system design.

Nomenclature

B_{K_V}	=	Motor speed constant parameter
B_{E_B}	=	Battery energy density
B_{I0}	=	No-load current parameter
B_{P-M}	=	Maximum power to mass ratio
B_{Ra}	=	Internal resistance parameter
c	=	Chord
C_d	=	Blade cross sectional drag coefficient

[1] Researcher, Faculty of Aerospace Engineering, ohadg@aerodyne.technion.ac.il , AIAA Member
[2] Professor, Faculty of Aerospace Engineering, rosen@aerodyne.technion.ac.il, AIAA Fellow

C_D, C_L	=	Vehicle's drag and lift coefficients, respectively
$C_{L\max}$	=	Vehicle's maximum lift coefficient
E_B	=	Battery energy capacity
g	=	Gravity acceleration
K_V	=	Motor speed constant
I_0	=	Motor no load current
I_{in}	=	Driver input current
m_0	=	Vehicle mass without the propulsion system
m_B	=	Battery pack mass
m_M	=	Electric motor mass
m_{Total}	=	Total vehicle mass
M_{tip}	=	Blade tip Mach number
$P_{out-\max}$	=	Maximum motor output power
P_{in}	=	Electric system input power
P_{out}	=	Motor output power
r	=	Radial coordinate
R	=	Propeller radius
R_a	=	Motor resistance
ROC	=	Rate of climb
S_W	=	Wing area
t	=	Cross sectional thickness
T	=	Thrust
V_F	=	Airspeed
V_l	=	Loitering airspeed
V_{st}	=	Stall airspeed

V_{in} = Driver input voltage

W_a = Axial induced velocity

η_D = Driver efficiency

η_P = Propeller efficiency

$\eta_{P-ideal}$ = Ideal propeller efficiency

η_S = Electric system efficiency

ρ_a = Air density

$\bar{\sigma}$ = Maximal Von-Misses stress

Ω = Rotational speed

I. Introduction

Most of nowadays Unmanned Aerial Vehicles (UAV's) are used for reconnaissance and surveillance missions [1]. Considerable effort has been directed towards the development of small tactical UAV's, sometimes referred to as Mini or Micro UAV's [2],[3]. These vehicles are applied as tactical surveillance tools - used by soldiers for 'behind the hill' reconnaissance purposes. Most of these UAV's are equipped with electric motors that contribute to the simplicity of operation and reduce significantly their noise signature.

The propulsion system of these small UAV's (batteries, motor, propeller, etc.) accounts for as much as 60% of the vehicle's weight [4]. Therefore optimization of the propulsion systems is extremely crucial.

The electric propulsion system of a typical UAV includes the following components:

a. Propeller
b. Electric motor
c. Energy source
d. Gear-box (optional)
e. Driver
f. Wiring, plugs, and connectors
g. Cooling system (optional)

The paper will concentrate on the first three items (propeller, electric motor, and the batteries). Although the other components are important, usually the influence of the first three on the UAV's performance is by far more significant.

Most of the existing methods for propeller design are based on the well known work of Betz from 1919 [6]. Example of such a design is presented in Ref. [7]. This approach is based on optimizing the propeller's geometry, at a certain specific operating condition (a certain combination of: airspeed, altitude, and propeller rotational speed), such that

the power, which is required to obtain a certain propulsive force at these operating conditions, is minimized (or alternatively, the thrust produced by a certain power is maximized). An example of such a design is the propeller of Rutan's Voyager (the first nonstop, non-refueled flight around the world) [8].

Betz method considers only the aerodynamic efficiency of the propeller. It does not include structural considerations or the propeller's noise signature. Thus for a practical design of a propeller, while using Betz method, a serial design process is used. First the optimal aerodynamic propeller, having a maximum efficiency, is defined. Then this propeller is modified in order to fulfill other goals. Such a process has been used extensively [8]-[10]. The main disadvantage of such an iterative process is that it does not ensure that the final design will be optimal.

The best approach for the complex design of propellers is to use Multidisciplinary Design Optimization *MDO* [11],[12]. During *MDO* all the different design goals and constraints are addressed simultaneously. Thus the "best" compromise between contradictory design goals will be reached. This kind of approach has been already applied to rotary wing designs. Most of the previous investigations were limited to two disciplines: either aerodynamic and structural analyses, mostly for helicopter rotors [13],[14], or aerodynamic and acoustic design of propellers [15]-[20]. Most of the previous investigations used a very limited number of design variables rather than the full range of design parameters that are under the authority of the designer. Previous investigations also included a limited number of constraints, and did not consider the entire propulsion system, namely the coupled system: propeller, gearbox, engine, and energy source [21]. Recently, a new comprehensive MDO design tool for propeller based propulsion systems was presented by the authors, that offers a very high flexibility in choosing the cost function, design variables and constraints [5],[22].

The design of various electric Mini-Unmanned Air Vehicles (UAV's) has been described in the past [3]-[4], [23]-[30]. Most of these articles discuss the design considerations of the various components, and the integration of these components into the final design.

It is clear from previous studies on electric UAV's, as well as other propeller based propulsion systems, that an optimization of the electric propulsion system of a UAV should include a simultaneous consideration of the: propeller, electric motor, and battery. The performance and characteristics of the vehicle depend on the strong interaction between these three.

The purpose of the present study is not to present an optimal design of a specific electric propulsion system for a certain UAV, but rather to investigate trends and obtain insight into the interactions between the various components

of the system. In order to do that, theoretical models of these components are required. While the propeller model of the present study is based on the well known blade-element/momentum theory, special effort is directed into modeling the electric motor and battery. These models are based on a comprehensive investigation of existing motors and batteries, followed by derivations of representative models that include certain parameters. All the various models are combined with various optimization schemes to form a comprehensive MDO tool that can handle a large number and variety of design variables and constraints. There is also a large flexibility in choosing the cost function, namely the goal of the design.

The new MDO tool is used in order to study optimal propulsion systems, for different design goals (cost functions) and constraints. The interaction between the various components of the system is investigated, explained, and discussed.

As indicated above, the analytical models of the electric motor and battery represent typical existing technologies. Yet, these technologies exhibit significant variations between products and a continuous rate of improvement. Thus the paper also includes a sensitivity study in order to understand how variations in the characteristics of the various electric components, can affect the system optimal design.

II. Analysis Tools

The following analysis tools are used to model the components of the entire propulsion system:

1. Propeller's aerodynamic model.
2. Propeller's structural model.
3. Electric motor model
4. Battery model

The selection of each model is based on the following two considerations:

1. It should be sufficiently accurate.
2. It should be efficient since the optimization procedure includes a very high number of iterations.

The aerodynamic model calculates the distribution of the aerodynamic loads along the propeller blades. This data is used in order to calculate the propeller's thrust and required power. In addition, the distribution of the aerodynamic loads is used as an input for the structural analysis. In the present case a Momentum/Blade-Element model is used. For regular flight conditions of propellers (uniform axial flow at high enough advance ratios) the blade's cross-sections do not experience stall and the Momentum/Blade-Element model gives results of good accuracy [31]. The

Blade-Element/Momentum analysis can be extended to include the influence of rotation on the aerodynamic behavior of cross-sections experiencing stall [32]. Momentum/Blade-Element models are usually much more efficient than other models, thus they are suitable for the present purpose.

A structural analysis is essential in order to ensure that the propeller blades will be able to withstand the aerodynamic and inertial loads that act along them. Common tools for the structural analysis of blades are Finite Element Models [33]. In order to reduce the computations, a more efficient rod model, together with a transfer-matrix formulation, is used [34]. The rod structural model describes the propeller blades as a series of straight segments, located along the blade's elastic axis. The structural cross-sectional properties are uniform along each segment and equal to the structural properties of a representative cross-section of that segment. The transfer matrix formulation is applied using the boundary conditions of a cantilevered rod (clamped root and free tip). The solution procedure is very efficient and the results are very accurate [34].

A. Electric Motor Model

Characteristics of 250 *BLDC* (Brush Less Direct Current) electric motors were analyzed. The list includes 12 manufacturers that are divided into three main groups:

I. Manufacturers of heavy duty/high voltage electric motors.

II. Manufacturers of high performance industrial electric motors.

III. Manufacturers of aeromodel/hobby electric motors.

Heavy duty motors are characterized by low speed and high torque. On the other hand, aeromodel motors exhibit high speed and low torque.

There is a relation between a motor maximum output power and its size/weight [35]. Figure 1 presents motors' maximum continuous power, $P_{out-\max}$, versus their mass, m_M. Each manufacturer is presented by a different symbol (there are 12 different symbols). In addition each symbol indicates to which group (of the above mentioned three groups) this manufacturer belongs:

I. Heavy duty – Solid symbols

II. High performance – Empty symbols

III. Aeromodel - 'Cross' (+) or 'Ex' (x)

Figure 1 also presents representative boundaries between these three groups. As indicated above, heavy duty motors exhibit low power to weight ratio, while aeromodel motors exhibit high power to weight ratio. It is the goal of any

air vehicle to exhibit high power to weight ratio, thus aeromodel motors are natural candidates for UAV's applications. Yet, UAV's motors are required to present much better reliability and endurance, than hobby motors. This aspect, as well as experience with existing UAV's motors, leads to the conclusion that group II is a better representative of UAV's motors.

The motor model of the present study will assume a constant maximum power to mass ratio, B_{P-M} [35]:

$$P_{out-\max} = B_{P-M} \cdot m_M \tag{1}$$

In region II, B_{P-M} vary between the following limits:

$$110\left[\frac{W}{kg}\right] < B_{P-M} < 800\left[\frac{W}{kg}\right] \tag{2}$$

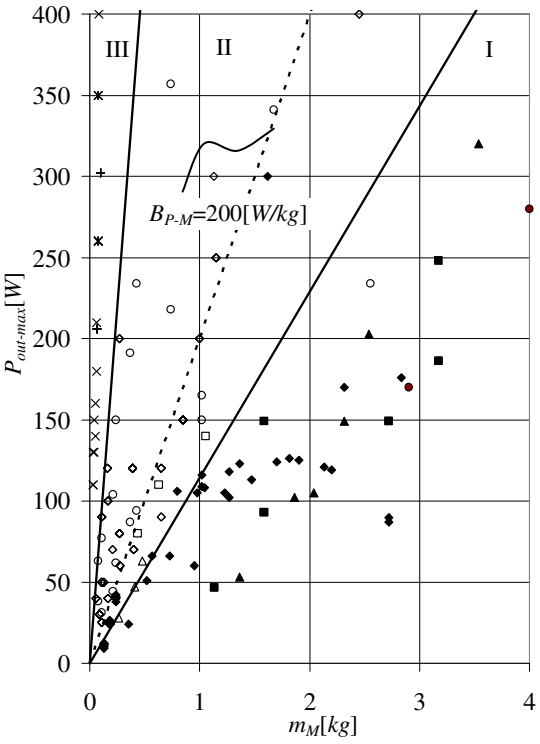

Figure 1- Motor maximum output power as a function of motor mass

Equation (2) presents a very wide range of variation of B_{P-M}. Examination of the data in Figure 1 shows that for a certain series of products, of the same manufacturer, different sizes of motors follow Eq. (1).

The differences in B_{P-M} between manufacturers, or between different series of the same manufacturer, probably emerge from different: technologies, design concepts, or manufacturing methods. For the present study a typical value of $B_{P-M} = 200[W/kg]$ will be used.

During the present study electric motors will be described by a simple performance model [36], which is based on the following assumptions:

a. Power factor is equal to unit. This assumption is applicable to small brushless Permanent Magnet (*PM*) motors [37].

b. Magnetic losses (eddy/Foucault Current and magnetic hysteresis) can be neglected.

Using these assumptions, the driver input power, P_{in}, and shaft output power, P_{out}, are given by the following expressions:

$$P_{in} = V_{in} \cdot I_{in} \tag{3}$$

$$P_{out} = (I_{in} - I_0) \cdot (V_{in} - I_{in} \cdot R_a) \tag{4}$$

I_{in} is the driver's input current, V_{in}, is the driver's input voltage, I_0 is the current at zero load, while R_a is the motor resistance.

The electric system efficiency, η_S, is:

$$\eta_S = \eta_D \cdot \left(1 - \frac{I_{in} \cdot R_a}{V_{in}}\right) \cdot \left(1 - \frac{I_0}{I_{in}}\right) \tag{5}$$

where η_D is the driver efficiency.

In the present study the driver efficiency is considered to be constant, $\eta_D = 0.95$.

The following relation also exists:

$$\Omega = (V_{in} - I_{in} \cdot R_a) \cdot K_V \tag{6}$$

where Ω is motor rotational speed and K_V is motor speed constant, which is identical to the inverse of torque constant or the inverse of back EMF (Electro Motive Force) constant.

The above described simplified model includes the following three motor parameters: speed constant, K_V, internal resistance, R_a, and no-load current, I_0. Simple relations between these three parameters will be used. These relations are based on available motors data.

The motor speed constant, K_V is directly related to the motor size. The torque constant (inverse of speed constant) depends on the motor flux linkage and magnetic circuit: the larger the motor, flux linkage and torque constant will also be larger. Consequently as the rotor becomes heavier the speed constant decreases. Figure 2 presents motor speed constant versus motor mass, for all the motors that were shown in Figure 1. Figure 2 also includes an internet database of electric aeromodel motors, which is available from the homepage of MotoCalc [38] software. This data base contains data for about 1300 electric motors which are mostly shown as a cloud of dots on the upper left side of the figure.

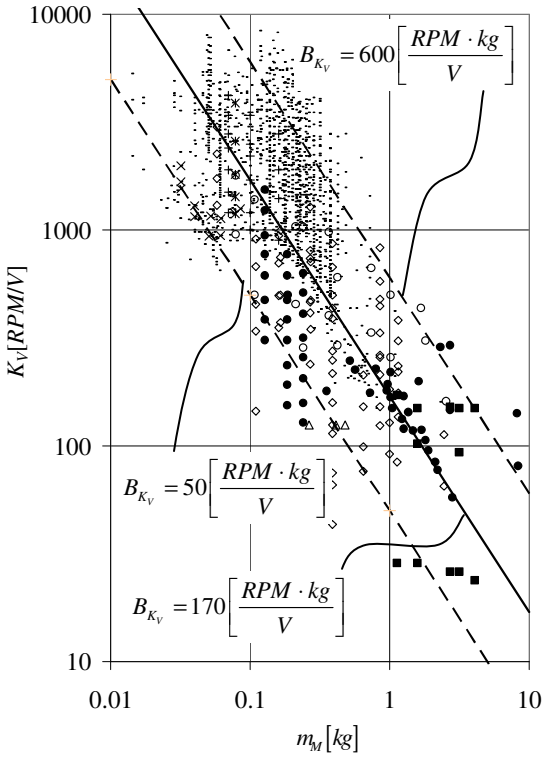

Figure 2- Speed constant as a function of motor mass

As indicated above, as motors become lighter, their speed constants become higher (heavy duty motors have low speed constants), thus a general relation can be described as follows:

$$K_V\left[\frac{RPM}{V}\right] = B_{K_V} / m_M\,[kg] \tag{7}$$

B_{K_V} is a speed constant parameter .For most cases it falls in between the following values(see Figure 2):

$$50\left[\frac{RPM \cdot kg}{V}\right] < B_{K_V} < 600\left[\frac{RPM \cdot kg}{V}\right] \tag{8}$$

For the present study a typical value of $B_{K_V} = 170\left[\frac{RPM \cdot kg}{V}\right]$ will be used (see Figure 2).

Motors' resistance versus motors' speed constants are shown in Figure 3. The following trend is clear: small aeromodel motors have low resistance, while heavy duty motors exhibit high resistance. In the present study the following relation is used (see Figure 3):

$$R_a[\Omega] = \frac{B_{Ra}}{\left\{K_V\left[\frac{RPM}{V}\right]\right\}^2} \tag{9}$$

B_{Ra} is internal resistance parameter that for most cases changes between the following values(see Figure 3):

$$2{,}500\left[\frac{V^2 \cdot \Omega}{RPM^2}\right] < B_{Ra} < 1{,}000{,}000\left[\frac{V^2 \cdot \Omega}{RPM^2}\right] \tag{10}$$

For the present study a typical value of $B_{Ra} = 60{,}000\left[\frac{V^2 \cdot \Omega}{RPM^2}\right]$ will be used (see Figure 3).

In the same manner Figure 4 presents motors no-load current, I_0, versus motors resistance, R_a. The following representative relation is used in the present study:

$$I_0[Amp.] = \frac{B_{I0}}{\left(R_a[\Omega]\right)^{0.6}} \tag{11}$$

B_{I0} is the no-load current parameter that for most cases changes between the following values(see Figure 4):

$$0.1\left[Amp. \cdot \Omega^{0.6}\right] < B_{Ra} < 0.4\left[Amp. \cdot \Omega^{0.6}\right] \tag{12}$$

For the present study a typical value of $B_{I0} = 0.2\left[Amp \cdot \Omega^{0.6}\right]$ will be used (see Figure 4).

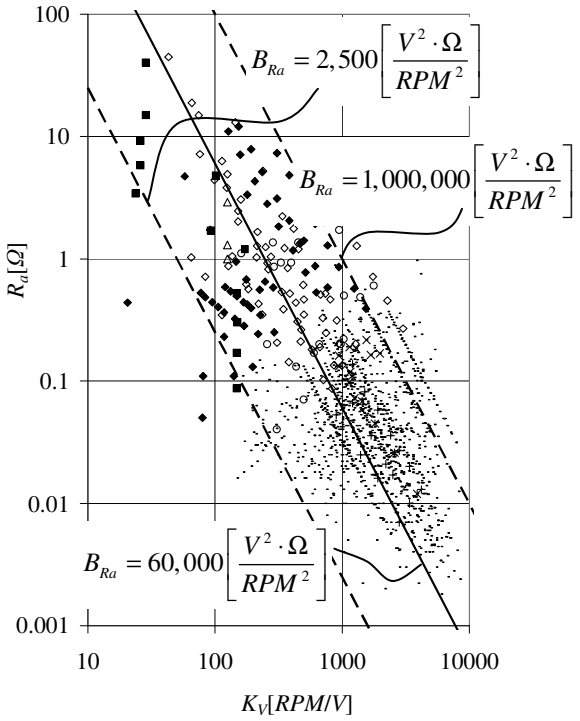

Figure 3- Internal resistance as a function of speed coefficient

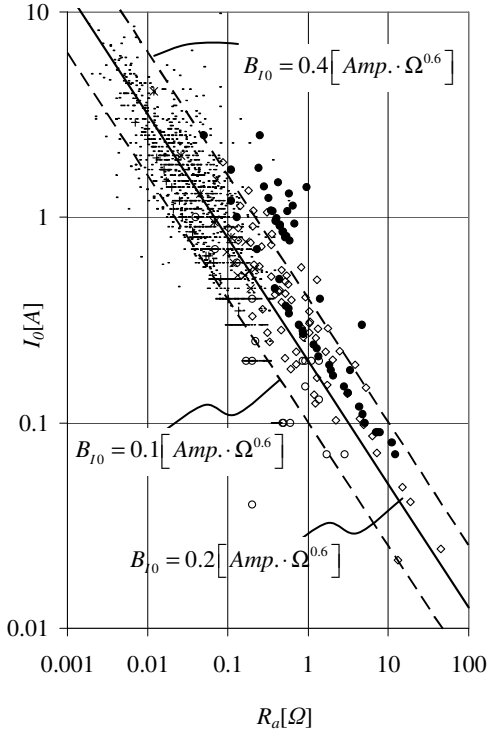

Figure 4- No load current as a function of internal resistance

B. Battery Model

An important component of an electric propulsion system is the battery pack. Often the battery represents one of the heaviest components of the entire vehicle [39]. One of the most common types of batteries is the Lithium Polymer (LiPo), which offers a high energy capacity along with low weight. Data of 240 LiPo batteries, produced by 11 different manufacturers, is presented in Figure 5. The figure shows batteries' energy capacity, E_B, as a function of the battery mass, m_B. The following representative relation between these two parameters is shown in Figure 5:

$$\mathrm{E}_B[W \cdot hr] = 4.04 \cdot \left(m_B[kg]\right)^2 + 139 \cdot m_B[kg] + 0.0155 \tag{13}$$

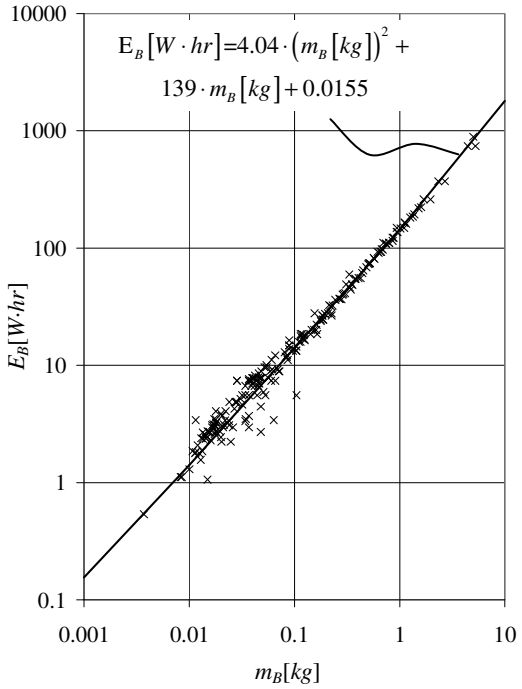

Figure 5- Battery capacity as a function of battery mass

III. Optimal Design of a Propulsion System

Any optimal design problem can be described mathematically as a search process for a design configuration that minimizes (or maximizes) a specific cost function, that represents the design goal. Usually this search process is carried out under certain design constraints.

Any design process requires an *a priori* definition of:

a. Design variables

b. Design constraints

c. Cost function

The design variables are parameters that are determined by the designer. In the general case of an electric propulsion system design, these variables are divided into five main categories:

a. Propeller's general design variables

b. Propeller's blade design variables

c. Blade's cross-sectional design variables

d. Electric motor design variables

e. Battery design variables

Propeller's general design variables affect the global configuration of the propeller system and may include the following parameters: number of propellers, number of blades, N_b , propeller radius, R , and rotational speed, Ω .

The blade's design variables are parameters that define the geometry and structure of each blade, namely the distribution along the blade of the following parameters: pitch angle, $\beta(r)$, chord, $c(r)$, sweep angle, dihedral angle (cone angle in the simplest case), mass and inertia, and structural properties.

The blade's cross-sectional design variables define the airfoil geometry as a function of a chord wise coordinate, thus for example [5]: If the cross-sections belong to the NACA-16 airfoil family [41], the geometry of each cross-section is defined by two parameters (that may vary along the blade):

a. Thickness ratio, $t/c(r)$

b. Design lift coefficient, $C_{l-i}(r)$

In the current study Clark-Y airfoils [42] are used, which are defined by the cross-sectional thickness ratio, $t/c(r)$.

The electric system variables include the motor mass, m_M, and the battery pack mass, m_B.

The design constraints may include for example: minimum or maximum chord size of the blade, allowable maximum stress, the system mass, motor maximum mass, etc.

The cost function is a quantitative measure of the success in achieving the design goal, thus the cost function offers a measure of the "quality" of the design.

A penalty method is used in order to solve the constrained optimization problem [43]. It leads to a new constrained cost function, which is minimized in order to find the optimal design, subject to all the constraints.

The present optimization scheme is based on a mixed strategy approach that combines different optimization methods:

a. Heuristic search– Simple Genetic Algorithm (SGA) [44]

b. Enumerative scheme – Nelder and Mead's Simplex scheme [45]

c. Derivative based scheme – Steepest Descent method [46]

This approach ensures a thorough search for the global minimum, by taking advantage of the strength of each of the above schemes. A detailed description of this strategy and examples of its application, are presented in Ref. [5].

It should be emphasized that this design approach is by no means "fully automatic". The designer plays a major role in the entire process. He or she, follows the results during the design procedure, and based on these results changes (if necessary) the optimization strategy. Thus, for example, at certain instance the designer may decide to ease certain constraints in order to increase the flexibility of the search process, or freeze a few variables in order to avoid impractical results.

IV. Design of an Optimal Propulsion System for an electric UAV

An electric Mini Unmanned Air-Vehicle (Mini-UAV) is considered. The mass of the vehicle without its propulsion system is $m_0 = 5.5[kg]$. The wing area is $S_w = 0.72[m^2]$, while the drag polar of the vehicle is described by the following equation:

$$C_D = 0.03 + 0.033 \cdot C_L^{\,2} \tag{14}$$

C_L and C_D are the vehicle's lift and drag coefficients, respectively.

A direct drive is used (the system does not include a gear box), namely the rotational speed of the propeller is equal to that of the electric motor, Ω.

Because of operational constraints, the radius of the propeller is limited:

$$R \le 0.15[m] \tag{15}$$

The blade tip Mach number, M_{tip}, is limited to subsonic speeds:

$$M_{tip} < 0.7 \tag{16}$$

As indicated above, Clark-Y cross-sections are used. The database for this airfoil family is limited to the following range of thickness ratios, t/c [42]:

$$0.04 < \frac{t}{c} < 0.21 \tag{17}$$

For practical reasons, the chord is also limited:

$$c/R < 0.35 \tag{18}$$

The design variables of the current design problem are:

a. Propeller radius, R

b. Distribution of chord length along the blade, $c(r)$

c. Distribution of pitch angle along the blade, $\beta(r)$

d. Distribution of thickness ratio along the blade, $t/c(r)$

e. Mass of the electric motor, m_M

f. Mass of the battery pack, m_B

The distribution of the various parameters along the blade is defined by their values at 11 radial stations, thus there are 36 design variables in total.

Although complex configurations of the blades (e.g. sweep and dihedral) may offer certain advantages [22],[47], the present study is confined to two-bladed propellers with straight blades and zero cone angles.

In the present study the electric motor mass and the battery pack mass cannot exceed 5[kg] and 20[kg], respectively:

$$m_M < 5[kg] \tag{19}$$

$$m_B < 20[kg] \tag{20}$$

The main task of the UAV is to loiter at low altitude above a certain area, thus the design goal is an optimal propulsion system for loitering conditions, that are defined by flight altitude (sea level in the present case) and airspeed, V_l. In the present case:

$$V_l = 1.2 \cdot V_{st} \tag{21}$$

where V_{st} is the vehicle's stall airspeed. The stall airspeed is a function of the maximum lift coefficient, $C_{L\max}$:

$$V_{st}^{\ 2} = \frac{(m_0 + m_M + m_B) \cdot g}{\frac{1}{2} \cdot \rho_a \cdot S_W \cdot C_{L\max}} \tag{22}$$

where g is the gravity acceleration. The maximum lift coefficient is $C_{L\max} = 1.4$.

Based on the vehicle's mass (which is a function of motor and battery mass), the stall and loitering airspeed are defined by using Eqs. (21) and (22). Then these flight conditions are used to calculate the required thrust, based on the vehicle's drag polar, Eq. (14).

According to Eq. (13) the battery energy capacity is a function of its mass. It is assumed in the present study that 70% of the total energy capacity is used for loitering, while the other 30% are used for: other flight phases (take off, climb, landing, etc.), payload requirements, and vehicle's subsystems.

A. Single Goal Design

As indicated above, the main task of the UAV is loitering. Thus a main design goal is to optimize loitering, namely maximize loiter time. On the other hand, since the vehicle is designed for tactical field operation, rate of climb after take-off represents a very critical parameter that is related to vehicles' survivability as well as safety of nearby people. Thus two different design goals are defined:

a. Maximum loiter time, t_l
b. Maximum Rate Of Climb (*ROC*) at loitering speed

As a first stage in this study, each of these goals will be dealt with separately as a single goal design.

For maximum loiter time, the cost function (to be minimized) is $-t_l$ (where t_l is loiter time). Similarly, for maximum rate of climb the cost function is $-ROC$ (where *ROC* is the rate of climb).

Figure 6 presents the optimal blade design for these two different cost functions. The figure presents the distribution of pitch angle, β, thickness, t, and chord, c, along the blade. The geometric characteristics of the two propellers are different; the pitch angle, chord length, and cross sectional thickness of the maximum *ROC* design are larger than the same parameters in the case of maximum loiter time design. This increase represents an effort to obtain maximum thrust in the case of maximum *ROC* design (the propeller rotational speed is limited because of tip speed constraint).

Important differences between the two optimal designs are evident from Table 1. The maximum *ROC* propulsion system has zero battery mass since maximum thrust is required in this case but there is no requirement for a finite flight time. On the other hand the maximum loiter time deign requires high energy capacity, thus the mass of the battery increases significantly but the vehicle's *ROC* at loiter is zero, which presents an impractical flight condition. Thus these two single goal optimal designs are impractical, yet they are important since they present the boundaries of practical designs and they offer important insight into design trends.

It should be noted (Table 1) that since the total masses of the two designs are different, there are significant differences in loiter speed between both cases (see Eqs. (21) and (22)). The battery of the maximum loiter time design does not reach the limit of 20[kg], since at a certain point an increase of the battery mass results in an increase in loiter speed and consequently an increase in vehicle's drag, that offset the beneficial effect of increasing the energy capacity.

Table 1 also presents the rotational speed, Ω, motor output power, P_{out}, propeller's thrust, T, and efficiencies of the propeller and the electric-system, η_P and η_S,, respectively. For each optimal design these parameters are given for two flight conditions: loiter and maximum *ROC*.

Propeller's efficiency is defined as follows:

$$\eta_P = \frac{T \cdot V_F}{P_{Out}} \tag{23}$$

It is interesting to note in Table 1 that for the maximum loiter time design, the flight conditions of loiter and maximum ROC are identical: At loiter the constraint on the maximum blade tip speed, Eq. (16), is active and does not allow any increase in power, thus resulting in zero *ROC*. On the other hand, for the design of maximum *ROC*, there are differences between the two flight conditions. While loitering is carried out at P_{out}=116[W], maximum *ROC* is obtained for P_{out}=1000[W] where the constraint of maximum blade tip speed becomes active again.

The efficiency of the propeller for maximum *ROC* is relatively low at that flight condition. Ideal propeller efficiency, $\eta_{P\text{-}ideal}$, is defined as the efficiency under the following ideal conditions [48]:

1. Zero wake rotation
2. Zero cross-sectional friction drag, $C_d = 0$.
3. Uniform axial induced velocity

The relation between the ideal propeller efficiency, $\eta_{P\text{-}ideal}$, and the ideal propeller's required power (motor output power), P_{out}, becomes [48]:

$$P_{Out} = 2 \cdot \rho_a \cdot V_F^{\,3} \cdot \pi \cdot R^2 \cdot \frac{1-\eta_{P-ideal}}{\eta_{P-ideal}^{\,3}} \tag{24}$$

For the present case of P_{out}=1000[W] and V_F=15.1[m/sec], the ideal efficiency according to Eq. (24) is $\eta_{P\text{-}ideal}$=0.612 (compared to a non-ideal value of η_P=0.561). This indicates that if the power of the propeller is increased (in order to increase *ROC* in this case) and the radius is limited, efficiency may decrease significantly.

Table 1 - Single goal design – Results for maximum loiter time and maximum rate of climb designs

		Design for Maximum Loiter time	Design for Maximum ROC
	$t_l[sec]$	17,175	0
	$ROC[m/sec]$	0	4.876
	$m_M[kg]$	2.52	5.0
	$m_B[kg]$	19.4	0.0
	$m_{total}[kg]$	26.9	10.0
	$V_F[m/sec]$	24.8	15.1
Operation at loiter	$\Omega[RPM]$	15,160	6,780
	$P_{Out}[W]$	505	116
	$T[N]$	16.6	6.2
	η_P	0.815	0.808
	η_S	0.818	0.792
Operation at max. *ROC*	$\Omega[RPM]$	15,160	15,160
	$P_{Out}[W]$	505	1000
	$T[N]$	16.6	37.1
	η_P	0.815	0.561
	η_S	0.818	0.738

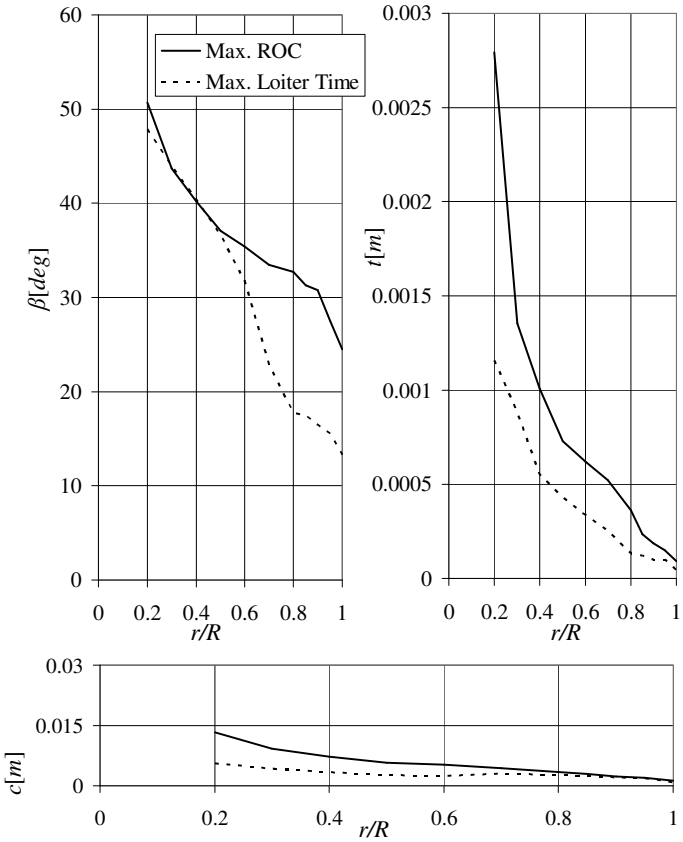

Figure 6- Single goal design - Geometry of maximum loiter time and maximum rate of climb propellers

The rotational speeds of the two designs, at loitering, are different. This difference is due to the difference in the loitering airspeed, V_l, a difference which is a result of the various vehicles' total mass, m_{total}, - see Eqs. (21),(22).

It should be pointed out that both designs have a radius of 0.15m, the maximum allowed value. This trend continued along the entire present study and thus data about the propeller radius is not repeated in what follows.

B. Dual Goal Design

A practical design presents a compromise between the two extreme and impractical design goals of sub-section A. This case of dual goal design leads to a multi objective optimization problem. In this case a Pareto front of the cost function can be drawn. This Pareto front is obtained by defining maximum loiter time as the goal, under specific *ROC* constraints. The two designs of Figure 6 represent the extreme right and left points of the Pareto front which is shown in Figure 7. This figure also presents the mass breakdown. As indicated above (Table 1), battery mass is high for long endurance and low *ROC*, while for short endurance and high *ROC* battery mass decreases significantly and the motor mass reaches its maximum value. The limit of the motor mass (5[kg]) is reached for *ROC* =2[m/sec], and for larger values of *ROC* the motor mass remains unchanged. As indicated above, the battery mass does not reach its limit (20[kg]) and only gets close to it for the maximum endurance design. Still, the battery mass exceeds the basic vehicle mass, m_0, for *ROC* close to 3.5[*m/sec*], which means that for most of the range of *ROC*, the battery mass represents a significant portion of the total vehicle mass.

Figure 8 presents the propeller's efficiency at the maximum *ROC* operating conditions. The ideal efficiency according to Eq. (24) is also shown. The actual efficiency is lower by approximately 0.06 compared to the ideal value.

C. Dual Goal Design under Mass and Structural Constraints

In order to make the design more practical the total mass of the vehicle is limited to 8[kg]. This limit is based on a typical weight that can be carried by a single soldier.

$$m_{total} \le 8[kg] \tag{25}$$

This means that the total mass of the propulsion system (motor and battery pack) cannot exceed 3[kg].

Table 2 and Figure 9 present the data and geometry of the two single goal designs: maximum *ROC* and maximum loiter time, under a total mass constraint (without additional constraints).

In general cross-sectional pitch angles of the maximum loiter time design are higher than the maximum *ROC* design. This reflects the difference in rotational speed. The two designs have to produce the same thrust at loiter (the total

vehicle's mass is the same), thus since the rotational speed of the maximum loiter time design is lower than that of the maximum *ROC* design, the pitch angle of the first one increases.

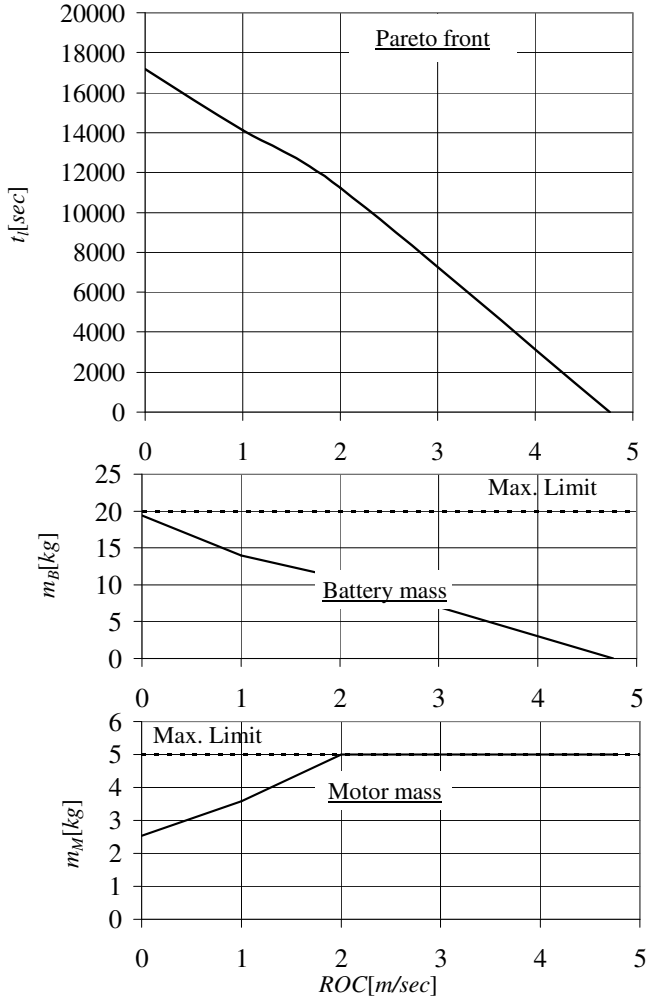

Figure 7- Dual goal design - Pareto front and mass breakdown

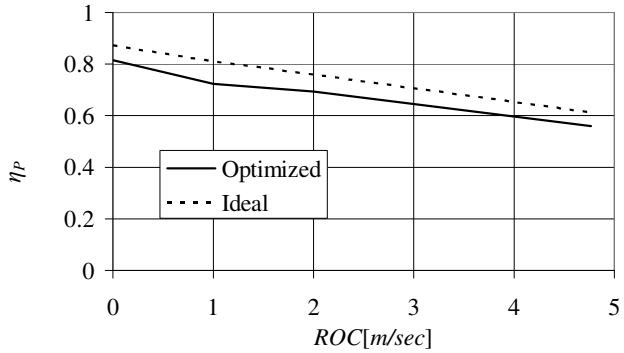

Figure 8- Dual goal design - Propeller's efficiency at maximum *ROC* operating condition

Table 2- Single goal design under total mass constraint - Results for maximum loiter time and maximum rate of climb designs

		Design for Maximum Loiter Time	Design for Maximum ROC
	$t_l[sec]$	9,750	0
	$ROC[m/sec]$	0	3.63
	$m_M[kg]$	0.41	3.0
	$m_B[kg]$	2.59	0.0
	$m_{total}[kg]$	8.0	8.0
	$V_F[m/sec]$	13.5	13.5
Operation at loiter	$\Omega[RPM]$	9,700	7,360
	$P_{Out}[W]$	81.5	82.5
	$T[N]$	4.94	4.94
	η_P	0.820	0.810
	η_S	0.812	0.820
Operation at max. *ROC*	$\Omega[RPM]$	9,700	15,150
	$P_{Out}[W]$	81.5	600
	$T[N]$	4.94	25.9
	η_P	0.820	0.584
	η_S	0.812	0.802

One of the characteristics of the optimal designs in Figure 9 is their very small chord and thickness at the outer cross sections of the blades. Such designs may not comply with structural requirements [5], thus structural constraints should also be considered.

It is assumed that the blade is made of Aluminum 7075-T6. The yield stress of this material is $5.03 \cdot 10^8 \left[Pa \right]$. The maximum Von-Misses stress, $\bar{\sigma}$, will be limited to:

$$\bar{\sigma} < 1.5 \cdot 10^8 \left[Pa \right] \tag{26}$$

The stress constraint is calculated for the maximum *ROC* conditions, which represent an extreme flight condition from the point of view of loads that act on the blades.

Figures 10 and 11 present comparisons between optimal designs, with and without structural constraints, for maximum *ROC* and maximum loiter time, respectively. The application of structural constraints increases significantly the chord length and thickness of the blades.

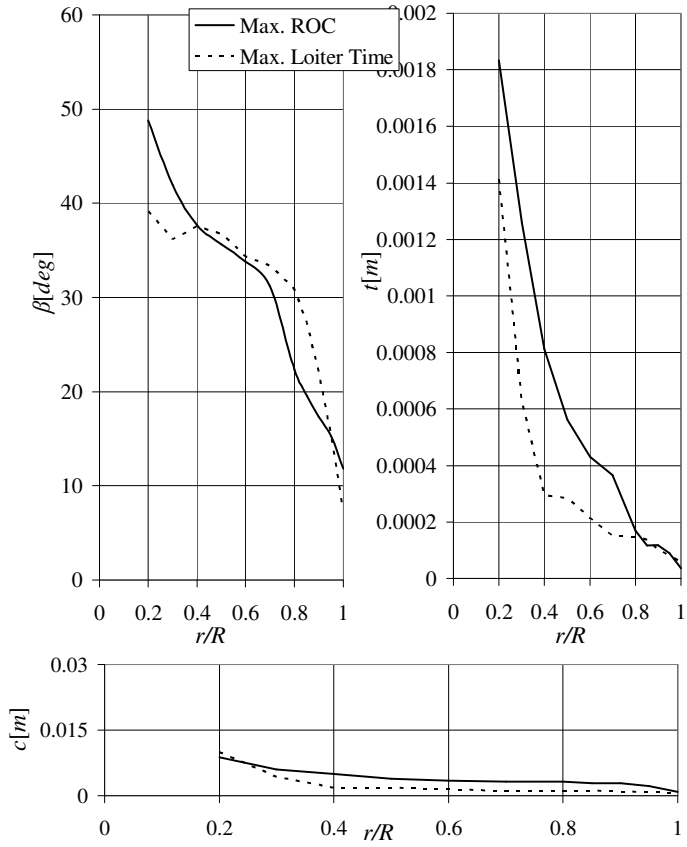

Figure 9- Single goal design under total mass constraint - Propeller designs for maximum loiter time and maximum rate of climb

Still, after the application of the structural constraints, the chord length of the optimized blades is small – less than 3[mm] at the outer 30% of the blades' length for the maximum loiter time design, and less than 5[mm] at the outer 15% portion of the maximum ROC design. Although the two designs comply with the structural constraints (Eq. (26)), the blade geometry is impractical and will not comply with maintenance and operational constraints. Thus additional geometric constraints, limiting the minimum blade chord, are introduced:

$$c \geq 0.01[m] \tag{27}$$

Figures 10 and 11 also present the geometry of optimal blades under combined structural (Eq. (26)) and geometric (Eq. (27)) constraints. Tables 3 and 4 present the characteristics of these two designs under the various constraints. It should be noticed that the introduction of structural constraints leads to a significant reduction of rotational speed of both designs, in order to keep stresses within their limit. Adding geometric constraints decreases the rotational speed even further: Wider and thicker blades result in larger centrifugal forces, thus a further reduction of the rotational

speed is needed. The decrease of the rotational speed results in a decrease of the available thrust at maximum *ROC* (for the optimal design of that flight condition) and thus a reduced *ROC*. In the case of maximum loiter time design; the reduction in rotational speed is accompanied by a reduction in the efficiencies of the propeller and electric system. This leads to a reduction in loiter time.

Figure 12 presents the Pareto front and mass breakdown, of the dual design case under a total mass constraint, and various combinations of other constraints. Naturally, and similar to the results that were shown in Figure 7, as the *ROC* increases loiter time decreases. The influence of adding structural constraints is a reduction of about 5% of loiter time, with a negligible influence on the mass breakdown. The influence of adding geometric constraints is an additional 5% reduction of loiter time and still a negligible influence on the mass breakdown.

According to Figure 12, loiter time and mass breakdown of the three designs are very similar, thus it can be concluded that the addition of structural and geometric constraints results in only a relatively small reduction of loiter time.

The last conclusion can be explained by examining the axial induced velocity, W_a, and the spanwise loading distribution, dT/dr, of the different optimal designs under the various constraints. Figure 13 presents comparisons between the maximum *ROC* designs. It is shown that the induced velocity and span wise aerodynamic loading distributions are very similar in all cases. As a result of applying structural constraints the maximum of the loading gets closer to the blade root in order to reduce the bending moment at the root. Adding geometric constraints result in stronger blades and thus the maximum of the aerodynamic loading occurs closer to the blade's tip. Similar trends, as a result of adding various constraints, also appear in the case of maximum loiter time designs.

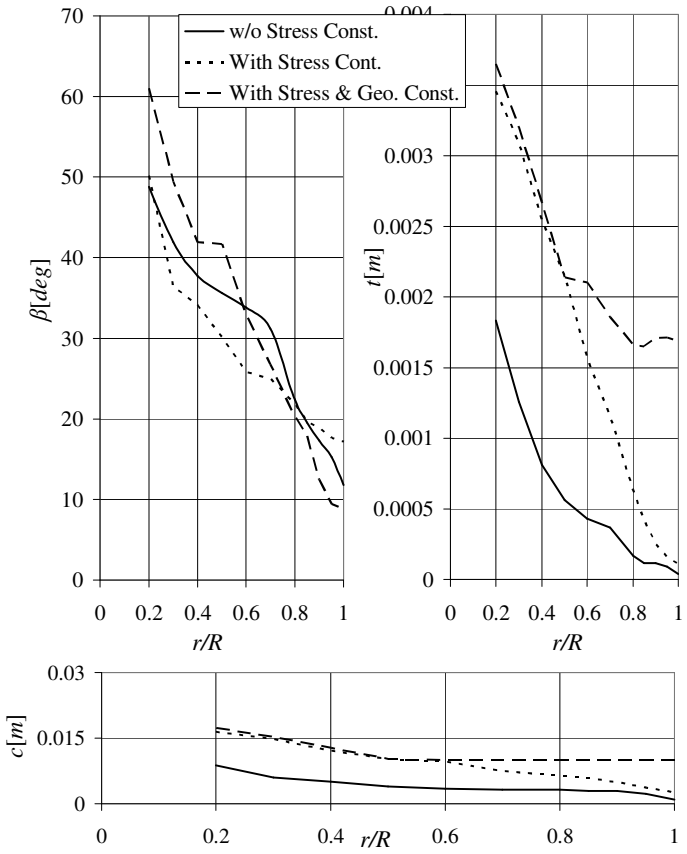

Figure 10- Maximum ROC design under total mass constraint - Influence of structural and geometric constraints

Table 3- Maximum ROC design under total mass constraint – The influence of additional constraints

		w/o additional constraints.	With Structural Const.	With Structural & Geo. Const.
	$t_l[sec]$	0	0	0
	$ROC[m/sec]$	3.61	3.54	3.45
	$m_M[kg]$	3.00	3.00	3.00
	$m_B[kg]$	0.00	0.00	0.00
	$m_{total}[kg]$	8.0	8.0	8.0
	$V_F[m/sec]$	13.5	13.5	13.5
Operation at loiter	$\Omega[RPM]$	7,360	5,780	4,961
	$P_{Out}[W]$	82.5	84.4	86.5
	$T[N]$	4.94	4.94	4.94
	η_P	0.810	0.791	0.773
	η_S	0.820	0.784	0.748
Operation at max. *ROC*	$\Omega[RPM]$	15,150	11,320	9,660
	$P_{Out}[W]$	600	600	600
	$T[N]$	25.9	25.4	24.9
	η_P	0.584	0.574	0.562
	η_S	0.802	0.723	0.668

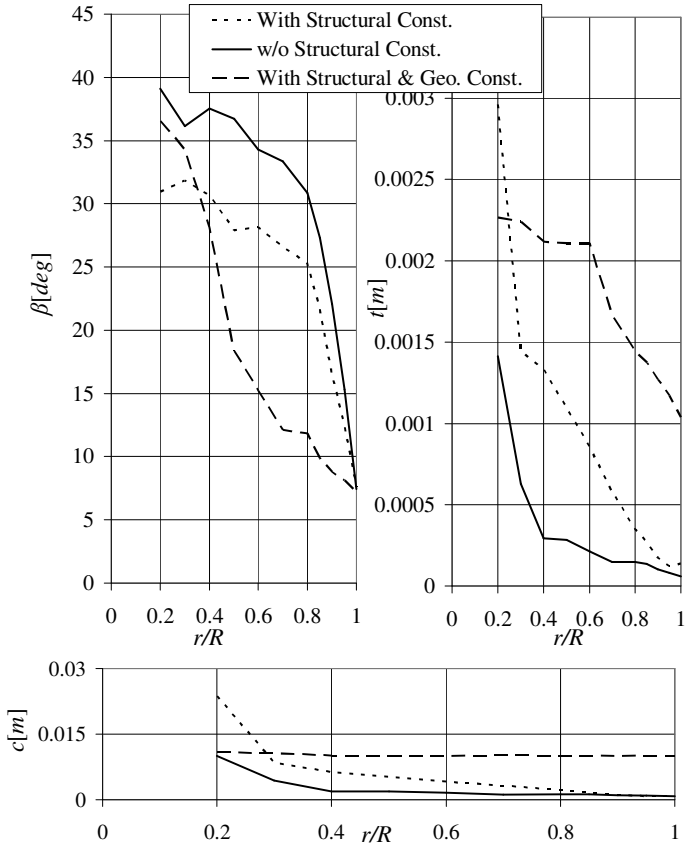

Figure 11- Maximum loiter time design under total mass constraint - The influence of additional constraints

Table 4- Maximum loiter time design with total mass constraint – The influence of additional constraints

		w/o Additional Const.	With Structural Const.	With Structural & Geo. Const.
	$t_l[sec]$	9,750	9,340	8,900
	$ROC[m/sec]$	0	0	0
	$m_M[kg]$	0.41	0.42	0.43
	$m_B[kg]$	2.59	2.58	2.57
	$m_{total}[kg]$	8.0	8.0	8.0
	$V_F[m/sec]$	13.5	13.5	13.5
Operation at loiter	$\Omega[RPM]$	9,700	7,800	6,890
	$P_{Out}[W]$	81.5	83.8	86.1
	$T[N]$	4.94	4.94	4.94
	η_P	0.820	0.797	0.775
	η_S	0.812	0.804	0.792
Operation at max. *ROC*	$\Omega[RPM]$	9,700	7,800	9,660
	$P_{Out}[W]$	81.5	83.8	86.1
	$T[N]$	4.94	4.94	4.94
	η_P	0.820	0.797	0.775
	η_S	0.812	0.804	0.792

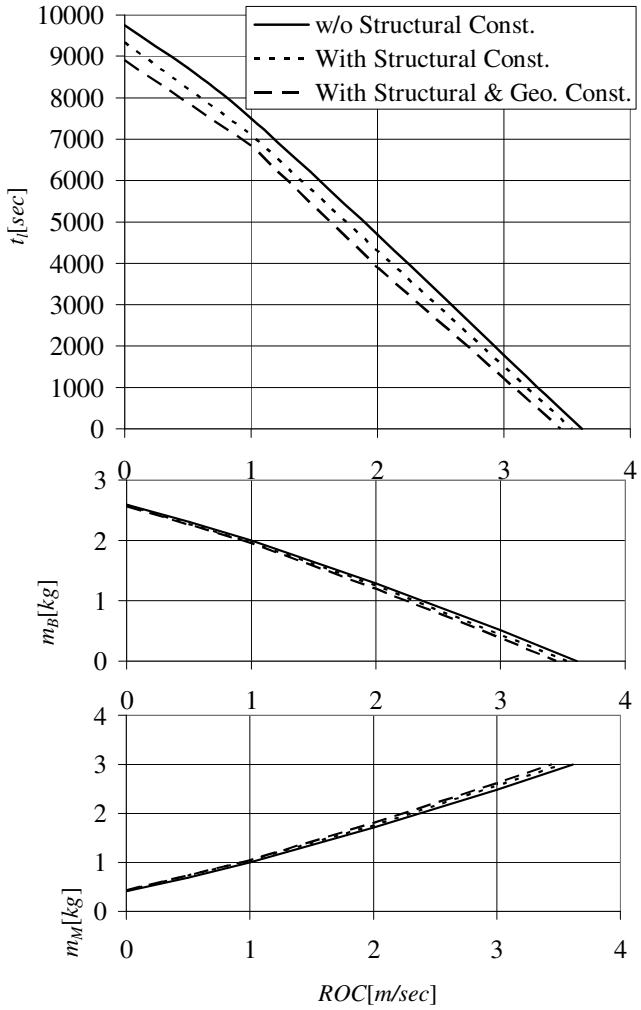

Figure 12- The influence of additional constraints on a dual goal design with total mass constraint - Pareto front and mass breakdown

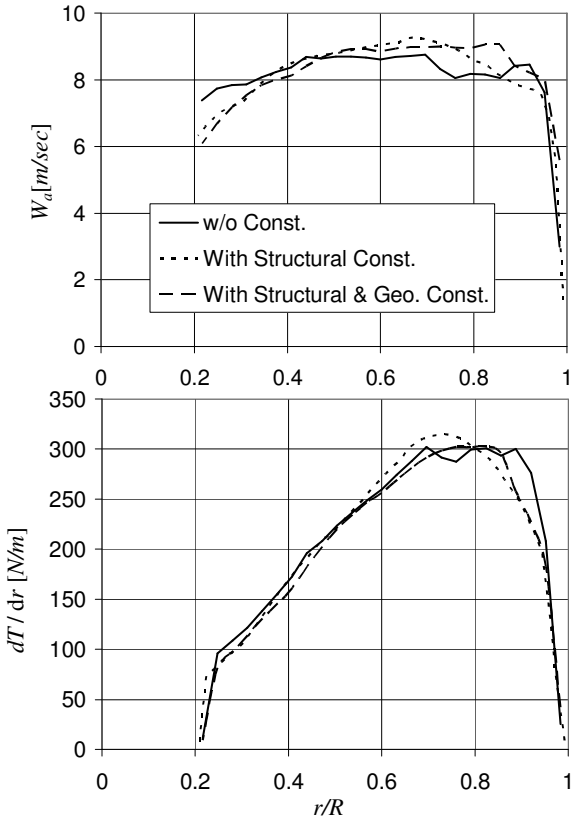

Figure 13- Maximum ROC designs – Span wise induced velocity and loading distributions

V. Sensitivity Study

The electric motor model includes four parameters:

a. $B_{P\text{-}M}$ - Maximum power to mass ratio

b. B_{Kv} - Speed constant parameter

c. B_{Ra} - Internal resistance parameter

d. B_{I0} - No-load current parameter

The battery is defined by the ratio between its energy capacity and mass – the energy density, B_{EB}

During the study of the previous section, nominal representative values of all these parameters were used. Yet, it was shown that there are significant differences between various motors. The purpose of the present section is to study the influence of these differences on the design and performance of the optimal propulsion system. The study will include variations of one of the parameters, while all the other parameters are constant and equal to their nominal values.

The design goal during this study is to maximize loiter time, while requiring minimal *ROC* of 2[m/sec], under the structural and geometric constraints of the previous section (Equations (25)-(27))

A. Maximum power to mass ratio, $B_{P\text{-}M}$

The first parameter to be investigated is the maximum power to mass ratio, $B_{P\text{-}M}$. This parameter has been varied between its limit values as defined by Eq. (2). The results are presented in Figure 14, where loiter time t_l, motor mass, m_M, and battery mass, m_B are presented as functions of the $B_{P\text{-}M}$. As expected, as $B_{P\text{-}M}$ increases loiter time increases too, since a reduction of the motor mass allows an increase of the battery mass. As $B_{P\text{-}M}$ increases, the rate of increase of loiter time with $B_{P\text{-}M}$ decreases .This is due to the fact that as the motor mass decreases, a large relative changes of the motor mass results in only a very small relative increase of the battery mass.

Since increase in $B_{P\text{-}M}$ means in many cases a reduction in reliability (aeromodel motors), the designer has to decide where the increase in loiter time due to $B_{P\text{-}M}$ increase does not worth the accompanied decrease in reliability.

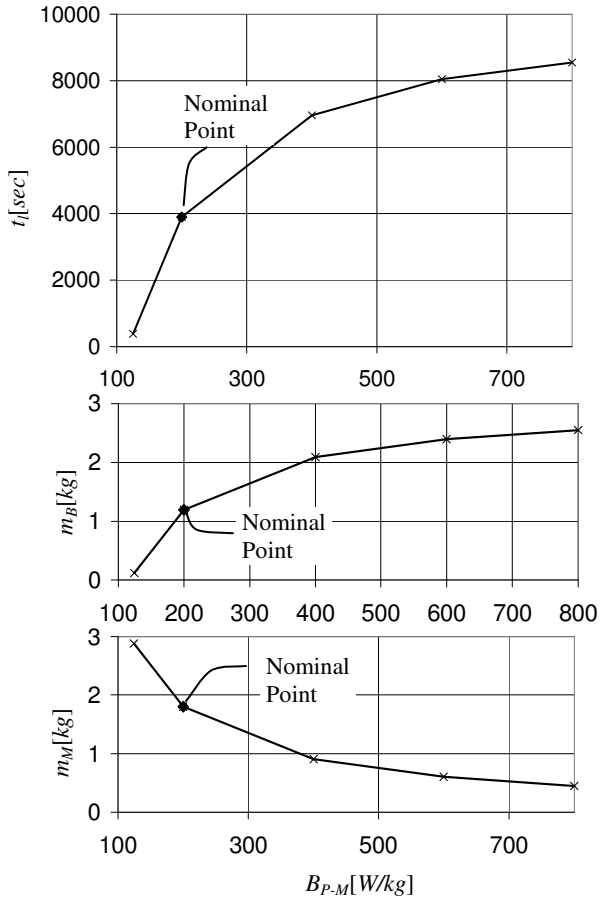

Figure 14- Loiter time and mass breakdown, as functions of maximum power to mass ratio ($B_{P\text{-}M}$)- Maximum endurance with ROC=2[m/sec]

B. Motor speed constant parameter, B_{Kv}

Another parameter that defines the electric motor characteristics is the motor speed constant parameter (see Eq.(7)). While the nominal value of this parameter in the previous examples was $B_{K_v} = 170\left[\frac{RPM \cdot kg}{V}\right]$, according to Eq. (8) its value may vary significantly.

Figure 15 presents loiter time and mass breakdown as functions of the speed constant parameter. The variations of the mass breakdown are negligible and loiter time varies by only 4% along the entire range. The influence of the motor speed constant parameter on the optimal blade design is also negligible, while the main influence is on the rotational speed. Figure 16 presents the rotational speed of the propeller at two flight conditions: loiter and *ROC*=2[*m/sec*]. In both cases as B_{Kv} increases the rotational speed increases too. Still the variations do not exceed 10% along the entire range of B_{Kv}..

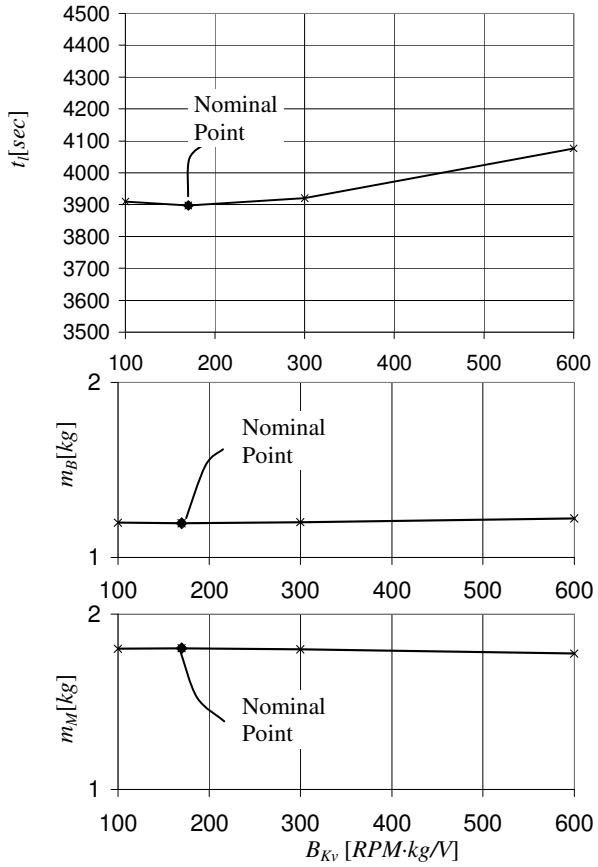

Figure 15- Loiter time and mass breakdown as functions of motor speed constant parameter (B_{Kv}) - Maximum endurance with *ROC*=2[m/sec]

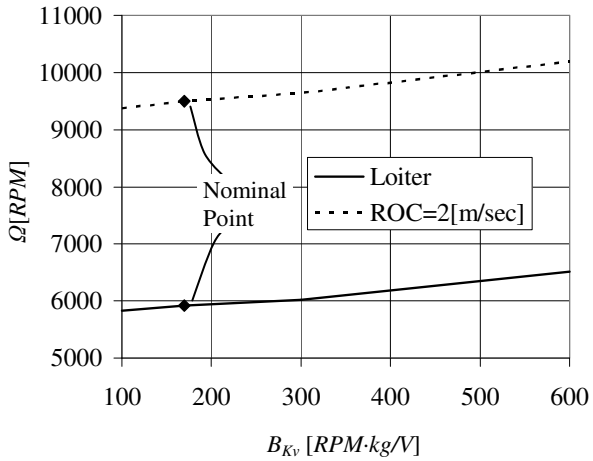

Figure 16- Propeller rotational speeds at loiter and ROC=2[m/sec], as functions of motor speed constant parameter, B_{Kv}

C. Internal resistance parameter, B_{Ra}

The internal resistance parameter, B_{Ra}, is defined by Eq. (9). Figure 17 presents loiter time and optimal mass breakdown, as functions of the internal resistance parameter. According to this figure there is an optimal value of this parameter is 12,000[$V^2\Omega/RPM^2$] that gives maximum loiter time of 4220[*sec*]. Figure 18 presents the influence of B_{Ra} on the: internal resistance, R_a, no-load current, I_0, and electric system efficiency, η_E,(for both flight conditions: loiter and climbing). As B_{Ra} increases the internal resistance decreases and the no load current increases. According to Eq. (5), the efficiency of the motor increases as R_a and I_0 decrease, and vise versa. Thus as B_{Ra} increases the opposite trends of R_a and I_0 result in a point of maximum efficiency, leading to a maximum value of loiter time, as indicated above.

D. No load current parameter, B_{Io}

Figure 19 presents loiter time and optimal mass breakdown as functions of the no load current parameter, B_{Io}, that was defined by Eq. (11). The influence of this parameter on the optimal mass breakdown is negligible, while it results in variations of less than 10% in loiter time. Figure 20 presents the influence of B_{Io} on: internal resistance, R_a no load current, I_0, and electric system efficiency (at loiter and climbing). It is shown that the internal resistance is not affected by variations of the no load current parameter. On the other hand the no load current increases as a result of increasing B_{Io}. Thus, according to Eq. 5, as B_{Io} increases the system efficiency decreases and loiter time decreases as well.

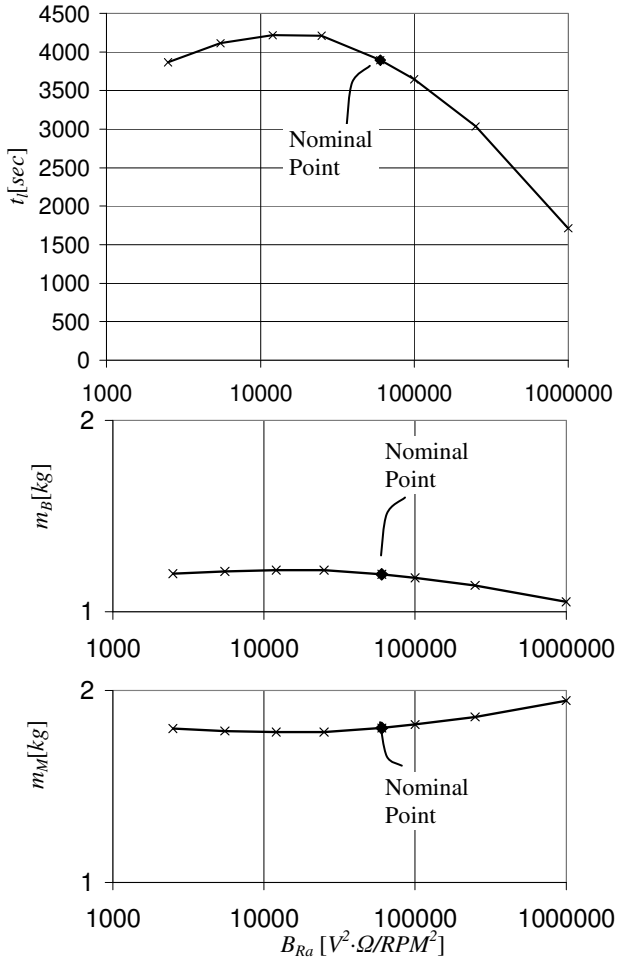

Figure 17- Loiter time and mass breakdown as functions of internal resistance parameter (B_{Ra}) - Maximum endurance with ROC=2[m/sec]

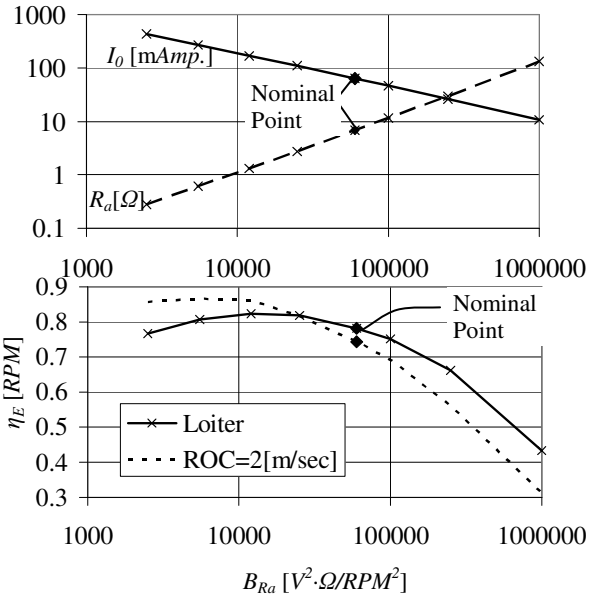

Figure 18- No load current, internal resistance, and Electric system efficiency at loiter and ROC=2[m/sec], as functions of internal resistance parameter , B_{Ra}

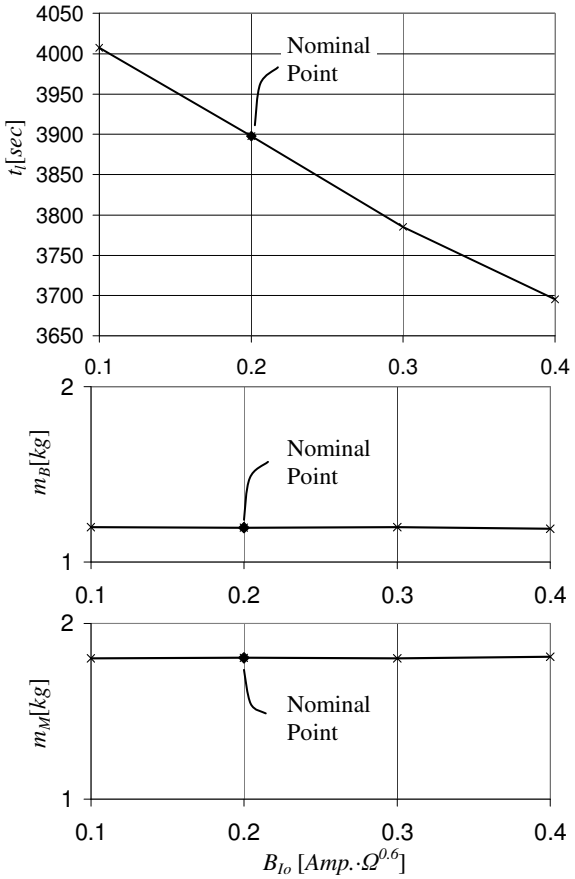

Figure 19- Loiter time and mass breakdown as functions of no load current parameter (B_{Io})- Maximum endurance with ROC=2[m/sec]

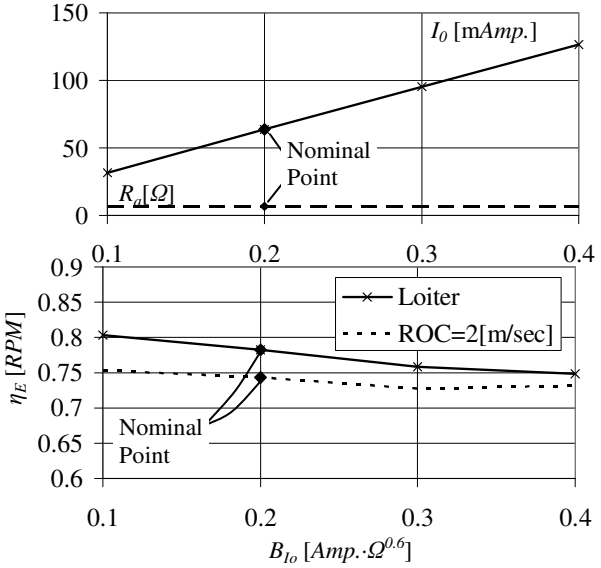

Figure 20- No load current, internal resistance, and Electric system efficiency at loiter and ROC=2[m/sec], as functions of internal resistance parameter , B_{Ra}

E. Battery's energy density, B_{E_B}

The model of LiPo batteries is given by Eq. (13). This model exhibits a very good agreement with existing batteries (see figure 5) with relatively small scatter. For the present sensitivity study, a linear model of variations about the nominal case is used:

$$\mathrm{E}_B\left[W\cdot hr\right]=\mathrm{B}_{E_B}\cdot m_B\left[kg\right] \tag{28}$$

B_{E_B} is the battery energy density (the energy per unit mass). A value of $B_{E_B}=180\left[W\cdot hr/kg\right]$ exhibits a good agreement with the curve of figure 5. During the years there has been a continuous, although fairly slow, improvement in the energy density of batteries. In the future, fuel-cells may offer $B_{E_B}>400\left[W\cdot hr/kg\right]$ [49] and up to $B_{E_B}=2300\left[W\cdot hr/kg\right]$ [50].

Figure 21 presents loiter time and optimal mass breakdown as functions of the energy density. It is shown that the mass breakdown is practically unaffected by variations of the energy density, while loiter time increases linearly with B_{EB}. The optimal blades design also is not affected by variations of the energy density of the battery.

VI. Summary and Conclusions

A comprehensive method for optimal design of electric propulsion systems for UAV's has been presented. The method is based on *MDO* approach that includes: aerodynamic, structural, electric, and performance analysis tools. These analysis tools are combined with three different optimization schemes in order to obtain the optimal design according to various design goals, using various design variables, and under various constraints.

While the aerodynamic and structural models of the propeller were presented elsewhere, the derivation of the electric motor model was presented in detail. This is a simplified model that is suitable for optimization, where large number of analyses is carried out and thus a numerically efficient model is required. This model includes four parameters that are defined based on examining a vast motor data from various manufacturers. A model of the energy capacity of the battery pack, as a function of its mass, is derived in a similar manner.

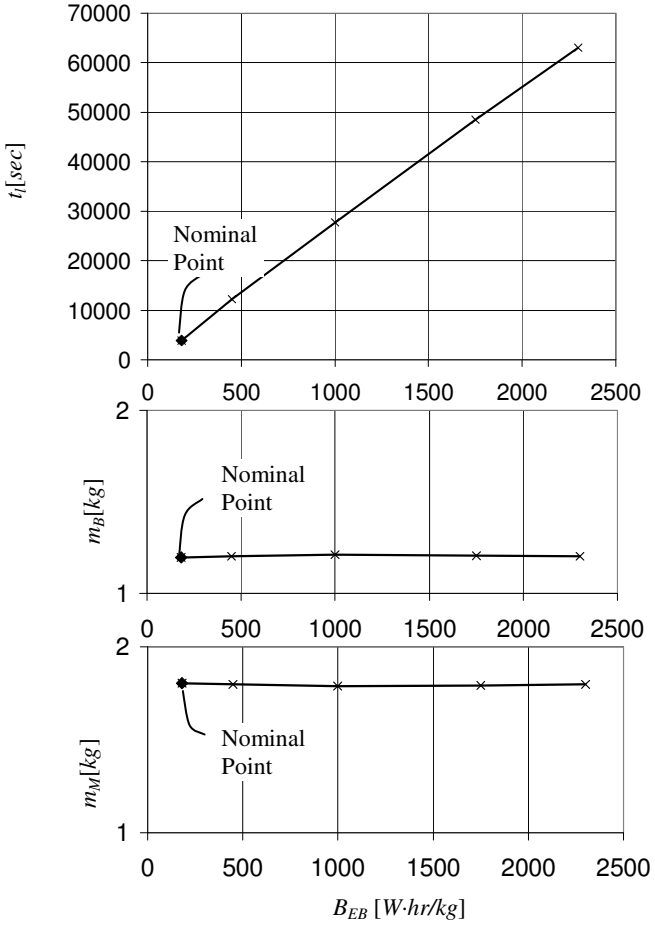

Figure 21- Loiter time and mass breakdown as functions of battery energy density (B_{EB}) - Maximum endurance with ROC=2[m/sec]

The new design tool was applied in order to design a propulsion system for an electric Mini-UAV. The design includes the propeller, motor and battery. There are two important performance indicators for this vehicle: Loiter time that is related directly to its main reconnaissance task and should be maximized, and rate of climb that is directly related to the survivability and safety of the vehicle. The study starts with single goal optimal designs of a propeller for maximum loiter time (that yields zero rate of climb because of propeller constraints), and a propeller for maximum rate of climb (that yields zero loiter time due to zero battery mass). The optimization is carried out with certain upper limits on the motor and battery masses. Although these two designs are impractical, they are important since they give an insight into the two extreme design trends. Thus for example, because the propeller radius is limited, maximum rate of climb results in relatively low propeller efficiencies. In order to obtain the high thrust that is necessary for high rate of climb, the chord in this design is roughly twice as large as the chord of the propeller design for maximum loiter time.

More practical designs lie in between the two extreme impractical cases. These designs are shown by a Pareto front, representing propellers that yield maximum loiter time for changing rate of climb capabilities. As the required rate of climb increases, the engine mass increases and loiter time decreases. It is interesting to note the complex influence of motor and battery mass: Increase in motor mass improves rate of climb, increase in battery mass extends loiter time. Yet, increasing vehicle mass results in higher loiter and climb airspeeds, thus making these flight conditions less efficient.

If the battery and motor masses are not limited, the total vehicle mass becomes too large to be carried by a soldier, which is a common requirement from such tactical systems (Mini-UAV). Thus it becomes important to use comprehensive tools, like the present one, that allow the introduction of additional constraints like an upper limit on the total mass of the UAV.

The optimal designs that are obtained based on aerodynamic/performance considerations, result in very narrow and thin blades that are impractical when structural and maintenance aspects are considered. Thus structural constraints that impose upper limits on the stresses are added. Yet, even under structural constraints, the blades are still too thin and narrow. Thus geometric constraints that pose lower limits on the chord length are also added. It is interesting to note that inspite of the significant increase in the size of the blades' cross sections due to the introduction of these constraints, the design trends are unchanged. In addition the design goals, namely loiter time under minimum rate of climb constraint, are usually reduced by no more than 10%.

The introduction of structural and geometric constraints results in a significant reduction of the propeller rotational speed. Consequently the tension stresses due to centrifugal forces do not exceed the allowed levels. Moreover, the *MDO* process is also capable of reducing the bending moment at the root, due to aerodynamic loads, by moving the point of maximum loading towards the blade root.

There are differences in the characteristics of electric components between different manufacturers, different technologies and other reasons. A sensitivity study was carried out in order to study the influence of such variations on the optimal system design. The paper presents the influence of variations of four motor parameters: maximum power to motor mass ratio, motor speed constant parameter, internal resistance parameter, and zero load current parameter. In addition the sensitivity to the battery energy density is also examined.

Increasing the maximum power to motor mass ratio parameter, results in a beneficial effect of increasing loiter time. Yet, the rate of increase of loiter time reduces, as the motor mass decreases. Since a reduction of this parameter is

accompanied in many cases by a parallel reduction of the motor's reliability and availability, at a certain stage a further increase of the maximum power to motor mass ratio is worthless.

Variations of the motor speed parameter exhibit negligible effect on the mass breakdown. Also loiter time changes by less than 5% for the entire range of variations. The propeller rotational speed exhibits a somewhat larger change, resulting in only small changes of the optimal blades design.

There is an optimal value of the internal resistance parameter that maximizes the loiter time. Still, the reltive variation in loiter time and mass breakdown are small. This is also true for the no load current parameter which has a small influence on the system characteristics.

Increase of the battery energy density increases loiter time in a linear manner. Nevertheless, this change does not affect the mass breakdown.

It can be concluded, based on the sensitivity study, that the battery density and maximum power to mass ratio have the largest influences on the design and performance of the system. The other parameters have a relatively minor influence on the vehicle performance, but they may influence the optimal design.

The present study shows once more that while optimizing a propeller based propulsion system, it is essential to consider simultaneously all the components of this system: propeller, motor and energy source- as well as the vehicle's characteristics.

Acknowledgment

This research was supported by the Bernard M. Gordon Center for Systems Engineering at the Technion. The authors would like to thank the center for this support.

The authors would also like to thank Prof. Raul Rabinovici from Ben-Gurion University and Dr. Vladimir Grinberg from Bental Motion Systems, for their assistance with the development of the electric system model.

Reference

[1] U.S. Office of the Secretary of Defense (OSD), "Unmanned aerial vehicles roadmap 2000-2025", available on: www.globalsecurity.org, April 2001

[2] Ott J. and Biezad D., "Design of a tube-launched UAV", AIAA Paper 2004-6493, *AIAA 3rd "Unmanned Unlimited" Technical Conference, Workshop and Exhibit*, Chicago, Illinois, 20th-23rd September, 2004

[3] Nagel A., Levy D.E., and Shepshelovich M., "Conceptual aerodynamic evolution of Mini/Micro UAV", AIAA Paper 2006-1261, *44th AIAA Aerospace Sciences Meeting and Exhibit*, Reno, Nevada, 9th-12th January, 2006

[4] M.T. Keennon, J.M. Grasmeyer, "Development of the Black Widow and microbat MAVs and a vision of the future of MAV design", *AIAA/ICAS International Air and Space Symposium and Exposition: The next 100Y*, Dayton, Ohio, 14th-7th July 2003

[5] Gur O. and Rosen A., "Optimization of Propeller Based Propulsion System", *4th AIAA Multidisciplinary Design Optimization Specialist Conference*, Schaumburg, Illinois, 7th-10th April, 2008

[6] A. Betz, "Screw propeller with minimum energy loss (Schraubenpropeller mit geringstem energieverlust)", Translation from German by D.A. Sinclair, Translation Section, N.R.C. Library, Technical translation 736. Source: Nachr. Kgl. Ges. Wiss. Göttingen, Math.-Phys. Kl. (2), 1919, pp. 193-217

[7] C.N. Adkins and R.H. Liebeck, 1994, "Design of optimum propellers", *AIAA Journal of Propulsion and Power*, Vol. 10, No. 5, September – October, 1994, pp. 676-682

[8] Roncz G.J., "Propeller development for the Rutan Voyager", Society of Automotive Engineers, SAE-891034, *General Aviation Aircraft Meeting and Exposition*, Wichita, Kansas, 11-13 April, 1989

[9] Succi G. P., "Design of Quiet Efficient Propellers", SAE 790584, *SAE Business Aircraft Meeting*, April. 1979

[10] Patrick H., Finn W.R., and Stich K.C., "Two and three-bladed propeller design for the reduction of radiated noise", AIAA 97-1710-CP, *3rd AIAA/CEAS Aeroacoustics Conference*, Atlanta, GA, 12-14 May, 1997

[11] AIAA technical committee on Multidisciplinary Design Optimization (MDO), "White paper on current state of the art", AIAA Technical Committee, January 1991

[12] Sobieszczanski-Sobieski J. and Haftka R.T., "Multidisciplinary aerospace design optimization: survey of recent development", *Structural Optimization*, Vol. 14, 1997, pp. 1-23

[13] Bennet R.L., "Application of optimization methods to rotor design problems", *Vertica*, Vol. 7, No. 3, 1983, pp. 201-208

[14] Friedmann P., "Application of modern structural optimization to vibration reduction in rotorcraft", *Vertica*, Vol. 9, No. 4, 1985, pp.363-376

[15] Ormsbee A.I. and Woan C.J.,"Optimum acoustic design of free running low speed propellers", AIAA Paper 77-1248, *AIAA Aircraft Systems & Technology Meeting*, Seattle, Washington, 22-24 August, 1977

[16] Chang L.K. and Sullivan J.P., "Optimization of propeller blade shape by an analytical method", AIAA Paper 82-1125, *AIAA/SAE/ASME 18th Joint Propulsion Conference*, Cleveland, Ohio, 21-23 June, 1982

[17] Chang L.K. and Sullivan J.P., "Optimization of propeller blade twist by an analytical method", *AIAA Journal*, Vol. 22, No. 3, February 1984, pp. 252-255

[18] Miller J.C., "Optimally designed propellers constrained by noise", Ph.D. thesis, Purdue University, December 1984

[19] Miller J.C. and Sullivan P.J., "Noise constraints effecting optimal propeller designs", SAE-850871, *Society of Automotive Engineers, General Aviation Aircraft Meeting and Exposition*, Wichita, Kansas, 16-19 April, 1985, pp. 4.585-4.593

[20] Drack E.L. and Wood A.L., "Design and analysis of propellers for general aviation aircraft noise reduction", ICAS-98-5,11,3, *21st International Congress of Aeronautical Sciences*, Melbourne, Australia, 13-18 September, 1998

[21] Monk J.S.,"The aerodynamic design of an optimized propeller for a high altitude long endurance UAV", *23rd International Congress of Aeronautical Sciences*, Toronto, Canada, 8-13 September, 2002, pp. 5104.1-5104.9

[22] Gur O. and Rosen A., "Multidisciplinary design optimization of a quiet propeller", *14th AIAA/CEAS Aeroacoustics Conference (29th AIAA Aeroacoustics Conference)*, Westin Bayshore Vancouver, British Colombia, Canada, 5th-7th May, 2008

[23] Logan J.M., Chu J., Motter A.M., Carter L.D., Ol M., and Zeune C., "Small UAV research and evolution in long endurance electric powered vehicles", AIAA Paper 2007-2730, *AIAA Infotech @ Aerospace 2007 Conference and Exhibit*, 7-10 May, 2007

[24] Grasmeyer J.M. and Keennon M.T., "Development of the black widow micro air vehicle", AIAA Paper 2001-0127, 39th Aerospace Sciences Meeting and Exhibit, Reno, Nevada, 8-11 January, 2001

[25] Roberts C., Vaughan M., and Bowman W.J., "Development of a solar powered micro air vehicle", AIAA Paper 2002-0703, *40th Aerospace Science Meeting and Exhibit*, Reno, Nevada, 14-17 January, 2002

[26] Peterson B., Erath B., Henry K., Lyon M., Walker B., {Powell N., Fowkes K., and Bowman W.J., "Development of a micro air vehicle for maximum endurance and minimum size", AIAA Paper 2003-416, *41st Aerospace Science Meeting and Exhibit*, Reno, Nevada, 6-9 January, 2003

[27] Wu H., Sun D., and Zhou Z., "Micro air vehicle: configuration, analysis, fabrication, and test", *IEEE/ASME Transactions on Mechatronics*, Vol. 9, No. 1, March 2004

[28] Ott J. and Biezad D., "Design of a tube-launched UAV", AIAA Paper 2004-6493, *AIAA 3rd "Unmanned Unlimited" Technical Conference, Workshop and Exhibit*, Chicago, Illinois, 20-23 September, 2004

[29] Choi T.P., Soban D.S., and Mavris D.N., "Creation of a design framework for all-electric aircraft propulsion architectures", AIAA Paper 2005-5549, 3rd International Energy Conversion Engineering Conference, Sna Francisco, California, 15-18 August, 2005

[30] Soban D.S. and Upton E., "Design of a UAV to optimize use of fuel cell propulsion technology", AIAA Paper 2005-7135, *AIAA Infotech @ Aerospace 2005 Conference and Exhibit*, Arlington, Virginia, 26-29 September, 2005

[31] Gur O. and Rosen A., "Comparison between blade-element models of propellers", *48th Israel Annual Conference on Aerospace Sciences*, 27-28 February, 2008

[32] Gur O. and Rosen A., "Propeller performance at low advance ratio", *Journal of Aircraft*, Vol. 42, No. 2, March-April 2005, pp. 435-441

[33] Yamamoto O. and August R., "Structural and aerodynamic analysis of a large-scale advanced propeller blade", *Journal of Propulsion and power*, Vol. 8, No. 2, March-April, 1992, pp.367-373

[34] Rosen A. and Gur O., "A transfer matrix model of large deformations of curved rods", *48th Israel Annual Conference on Aerospace Sciences*, 27-28 February, 2008

[35] Hanselman D.C., "*Brushless permanent-magnet motor design*", McGraw-Hill, Inc. 191 p.

[36] Lawrence D.A. and Mohseni K., "Efficiency analysis for long-duration electric MAVs", AIAA Paper 2005-7090, Infotech @ Aerospace, Arlington, Virginia, 26-29 September, 2005

[37] Su G.-J., Adams D. J., "Multilevel DC link inverter for brushless permanent magnet motors with very low inductance", *IEEE IAS 2001 Annual Meeting*, Chicago, Illinois, 30 September – 5 October 5, 2001

[38] **http://www.motocalc.com**, cited: 1 June, 2008

[39] Logan M.J., Chu J., Motter M.A., Carter D.L., Ol M., and Zeune C., "Small UAV research and evolution in long endurance electric powered vehicles", AIAA Paper 2007-2730, *AIAA Infotech @ Aerospace 2007 Conference & Exhibit*, 7-10 May, 2007

[40] Reneaux J. and Thibert J-J., "The use of numerical optimization for airfoil design", AIAA Paper 85-5026, *AIAA 3rd Applied Aerodynamics Conference*, Colorado springs, Colorado, 14-16 October, 1985

[41] Borst V.H. and Associates, "Summary of propeller design procedures and data", US Army Air Mobility Research & Development Laboratory Technical Report No. 73-34A/B/C, (3 volumes), November 1973

[42] Korkan K.D., Camba J. and Morris P.M., "Aerodynamic data banks for clark-Y, NACA 4-digit, and NACA 16-series airfoil families", NASA Contract Report No. 176883, Januray 1986

[43] Boyd S. and Vandenberghe L., "*Convex optimization*", Cambridge University Press, 2004, 716 p.

[44] Goldberg E.D., "Genetic algorithms in search, optimization, and machine learning", Addison-Wesley Publishing Company, 1989, 412 p.

[45] Nelder J.A. and Mead R., "A simplex method for function minimization", *Computer Journal*, Vol. 7, 1965, pp.308-313

[46] Van der Velden A., "Tools for applied engineering optimization", AGARD R-803 AGARD-FDP-VKI special course at the VKI, April 1994

[47] Sullivan J.P., Chang L.K., and Miller C.J., "The effect of proplets and bi-blades on the performance and noise of propellers", SAE Paper 810600, *SAE Business Aircraft Meeting and Exposition*, Wichita, Kansas, 7-10 April, 1981

[48] Glauert H., "*Airplane propellers*" in "*Aerodynamic Theory*" (Vol. 4, Division L), F.W. Durand, (Ed.), New York, Dover, Third Edition, 1963

[49] Burke K. A. and Jakupca I., "Unitized regenerative fuel cell system gas storage-radiator development", NASA TM 2005-213442, October 2005

[50] Wicke G.B., "General motors hydrogen storage requirements for fuel cell vehicles", Argonne National laboratory, GM R&D and Planning DOE Hydrogen Storage Workshop August 14-15, 2002, **http://www1.eere.energy.gov/hydrogenandfuelcells/pdfs/h2_fuelcell_vehicles.pdf** Cited: August 2008